HHS Public Access

Author manuscript

Life Sci. Author manuscript; available in PMC 2022 February 28.

Published in final edited form as:

Life Sci. 2022 January 01; 288: 120182. doi:10.1016/j.lfs.2021.120182.

Blocking I—Ag^7 class II major histocompatibility complex by drug-like small molecules alleviated Sjögren's syndrome in NOD mice

Shivai Gupta[a], **Danmeng Li**[b], **David A. Ostrov**[b], **Cuong Q. Nguyen**[a,c,d,*]

[a]Department of Infectious Diseases and Immunology, College of Veterinary Medicine, University of Florida, Gainesville, FL, USA

[b]Department of Pathology, Immunology & Laboratory Medicine, College of Medicine, University of Florida, Gainesville, FL, USA

[c]Department of Oral Biology, College of Dentistry, University of Florida, Gainesville, FL, USA

[d]Center of Orphaned Autoimmune Diseases, University of Florida, Gainesville, FL, USA

Abstract

Background: Sjögren's syndrome (SjS) is an autoimmune disease with a strong genetic association. To date, no vaccine or therapeutic agent exists to cure SjS, and patients must rely on lifelong therapies to treat symptoms. Human leukocyte antigens (HLA) are primary susceptibility loci that form the genetic basis for many autoimmune diseases, including SjS. In this study, we sought to determine whether blocking MHC class II I—Ag^7 antigen presentation in the NOD mouse would alleviate SjS by preventing the recognition of autoantigens by pathogenic T cells.

Methods: Mapping of the antigenic epitopes of Ro60 autoantigen to I—Ag^7 of the NOD mice was performed using structural modeling and in-vitro stimulation. Tetraazatricyclo-dodecane (TATD) and 8-Azaguanine (8-Aza) were previously identified as potential binders to I—A^{g7} of the NOD mice using in silico drug screening. Mice were treated with 20mgs/kg via IP every day five days/week for 23 weeks. Disease profiling was conducted.

Findings: Specific peptides of Ro60 autoantigen were identified to bind to I—Ag^7 and stimulated splenocytes of the NOD mice. Treating NOD mice with TATD or 8-Azaguanine alleviated SjS symptoms by improving salivary and lacrimal gland secretory function, decreasing the levels of autoantibodies, and reducing the severity of lymphocytic infiltration in the salivary and lacrimal glands.

*Corresponding author at: Department of Infectious Diseases and Immunology, PO Box 110880, College of Veterinary Medicine, University of Florida, Gainesville, FL 32611-0880, USA. nguyenc@ufl.edu (C.Q. Nguyen).

Data sharing

Data from this manuscript are available from the corresponding author upon reasonable request.

CRediT authorship contribution statement

SG, CN, and DO conceived and designed the experiments and completed experiments. DL performed the in-silico modeling and docking. They analyzed all data and prepared the manuscript. All authors reviewed and approved the manuscript.

Declaration of competing interest

All authors have no competing interests.

Interpretation: This study presents a novel therapeutic approach for SjS by identifying small molecules capable of inhibiting T cell response via antigen-specific presentation.

Funding: CQN is supported financially in part by PHS grants AI130561, DE026450, and DE028544 from the National Institutes of Health.

Keywords

Sjögren's syndrome; Major histocompatibility complex; NOD mouse; Small molecules; Therapy

Research in context

Evidence before this study

There is currently no cure for SjS. 97% of patients report using eye drops, artificial tears, or non-prescription eye ointments for treatment. Patients only rely on an anti-inflammatory agent, disease-modifying anti-rheumatic drugs (DMARDs), Rituximab (anti-CD20), and corticosteroids. Other drugs like hydroxychloroquine (HCQ), methotrexate, and azathioprine have provided mixed results in clinical trials. Recent studies have demonstrated that small molecules targeting MHC in mice or HLAs in humans can prevent Graves' disease, multiple sclerosis, and Type 1 Diabetes. SjS is strongly associated with certain risk MHC/HLAs. However, no study has been conducted to determine whether targeting risk MHC/HLAs could alleviate SjS. Therefore, the goal of this study was to block MHC class II antigen presentation to prevent the autoimmune response in SjS.

Added value of this study

Herein, we documented two novel and significant findings. First, we mapped specific epitopes of a key Ro60 autoantigen to MHC class II I—A^{g7} of the NOD and confirmed their antigenic effect by eliciting T cell response. Second, using two previously identified small molecules TATD and 8-Aza bound to I—A^{g7}, we demonstrated for the first time that they could alleviate SjS symptoms by improving salivary gland secretory function, decreasing the levels of autoantibodies, and reducing the severity of lymphocytic infiltration in the salivary glands. These findings provide a feasible, achievable, and solid scientific premise to examine the therapeutic effects of blocking pathogenic T cell activation by autoantigen-MHC complexes using a rational in silico structure-based approach.

Implications of all the available evidence

The significant aspect of this study is that it should establish the direction forward for generating and testing an appropriate therapy for blocking antigen presentation. Using a rational in silico structure-based application to identify the potential binders that could interfere with specific antigen presentation will provide a novel approach by developing a personalized medical treatment for SjS patients based on specific high-risk HLAs without generating general immune deficiency.

1. Introduction

Sjögren's Syndrome (SjS) is a chronic, progressive, and systemic autoimmune disease associated with a drastic decrease in quality of life [1–4]. SjS is a debilitating disease affecting 3.1 million individuals in the US and features a highly skewed sex distribution (9:1) from women to men. It is characterized by lymphocytic infiltration in the salivary and lacrimal glands [5,6]. Approximately 50% of SjS cases overlap with a different autoimmune disease, of which the most common are rheumatoid arthritis and systemic lupus erythematosus [2]. Clinical symptoms include xerostomia, keratoconjunctivitis sicca, as well as skin and vaginal dryness. Additionally, various extra-glandular manifestations include chronic musculoskeletal pain, fatigue, and a higher risk of non-Hodgkin's lymphoma [7]. In addition to the dysfunction of exocrine glands, SjS also has other targets for systematic manifestations, including the skin, gastrointestinal tract, lungs, blood vessels, liver, pancreas, kidneys, and may affect the peripheral nervous system [8,9]. SjS is characterized by lymphocytic infiltrates in the exocrine glands, which include B and T cells, with distinct pathogenic roles in primary SjS immunopathology [10].

The effector T cells and their cytokines contribute significantly to different etiologies of the autoimmune process. Studies have shown increased interferon (IFN)-γ- and IL-17 in salivary glands and plasma of human and animal models of SjS [11–14]. Previous research in mice revealed that IFN-γ plays an early role in disease development by recruiting pathogenic lymphocytes to the salivary glands and delaying gland development [15,16]. Similar to murine models, SjS patients exhibit high levels of IFN-γ and IFN-responsive factors in sera and exocrine glands. The upregulation of the IFN pathway induces the proliferation of macrophages, natural killer (NK) cells, and $CD8^+$ T cells. In addition, Th17 cells have been shown to drive the inflammatory response by producing pro-inflammatory cytokines, inducing germinal center formation, and driving antibody response [11,12,17–20].

The activation of the effector helper T cells is mediated by antigen presentation via MHC class II molecules. There is significant evidence to suggest that MHC class II is strongly associated with the development of SjS [21–24]. The reported risk haplotypes differ slightly by phenotype and ancestral population, but a meta-analysis identified the DRB1*0301, DQA1*0501, DQB1*0201, and DRB1*03 alleles as risk factors for SjS while the DQA1*0201, DQA1*0301, and DQB1*0501 alleles were protective [25]. In a recent large-scale association study of Europeans, strong genetic associations of SjS with HLA-DRA, HLA-DQB1, and HLA-DQA1 at the 6p21 locus were confirmed [26]. Multiple independent HLA alleles have been identified that share a linkage with the disease, including the previously reported alleles HLA-DQA1*05:01, HLA-DQB1*02:01, and HLA-DRB*03:01. Within the Han Chinese population, two independent association signals at the 6p21.3 locus [26] corresponding to HLA-DRB1/HLA-DQA1, and HLA-DPB1/COL11A2 have been identified. HLA class II is associated with autoantibody production in SjS, as anti-Ro/SSA and anti-La/SSB are significantly increased in HLA-DQ1/HLA-DQ2 heterozygous patients [27] but not with other clinical features [28], and HLA DRB1*1501, but not DRB1*0301, are associated with anti-cyclic citrullinated antibodies (ACA) [29].

As alluded, autoantigens presented by antigen-presenting cells via MHC complex can initiate the autoimmune cascade and blocking this interaction could have a therapeutic effect. Recent studies have shown that interfering or blocking the HLA or MHC molecules, irrespective of the autoantigen, suppressed the immune cascade and alleviated several autoimmune diseases, specifically, type 1 diabetes, Graves' disease, and autoimmune thyroiditis [22–24]. Based on these studies, we hypothesized that inhibiting antigen presentation by targeting MHC class II can prevent the autoimmune response in SjS and provide therapeutic benefit by preventing recognition of the HLA/self-peptide complex by pathogenic T cells. To test this hypothesis, we selected two small molecules, tetraazatricyclo-dodecane (TATD) and 8-Azaguanine (8-Aza). These drugs were identified as potential binders to I—A^{g7} of NOD mice using in silico screening, in which TATD was determined to bind in vivo, and the blocking was determined as interference with T cell responses [21,22]. Female NOD mice were treated with TATD or 8-Aza. The results showed that both small molecules significantly reduced salivary/lacrimal inflammation, restored secretory function, and decreased the autoantibodies associated with SjS.

2. Materials and methods

2.1. Structural modeling and molecular docking

The crystal structure of the I—A^{g7} complexed with the three peptides selected corresponding PDB code 6BLX was used for modeling I—A^{g7} with the three peptides $Ro60_{323\text{-}332}$HVLIALETYR, $Ro60_{528\text{-}537}$ HPAVALREYR, and $Ro60_{270\text{-}279}$VEAEKLLKYL. The peptides were mutated using COOT [30] (Crystallographic Object-Oriented Toolkit UK) with rotamers representing a local energy minimum of torsional angles while ensuring Leucine and Tyrosine were in P6 and P9, respectively. The geometry of the resulting complex was regularized in PHENIX (Supported and distributed by NIH/NIGMS Program Project Grant (P01GM063210), NIH/NIGMS R24 National Resource Grant (R24GM141254) and the Phenix Industrial Consortium, USA) [31]. Autodock Vina (Scripps Research, USA) [32] was used for molecular docking after water and other atoms were removed, with no presence of peptide. Then, the positions with the lowest binding energy (ΔG) of TATD and 8-Aza were superpositioned with I—A^{g7} complexed with peptides using PHENIX. PyMOL (https://pymol.org/2/) was used to generate molecular graphic images.

2.2. Mapping of Ro60 epitopes to I—A^{g7}

The sequence of mouse Ro60 was obtained from UniProt KB–008848. The peptide sequence of MKRHGLDNYR in Harrison et al. [32] shows leucine (L) at position six and tyrosine (Y) at position nine based on the structure and presentation by I—Ag^7. When presented on the MHC I—Ag^7' the peptide indicates T cell receptor contact on the peptide while being presented by I—Ag^7 with the residues and L and Y acting as anchor peptides. Based on the composition of MKRHGLDNYR peptide, a manual search was carried out in the mouse protein Ro60 for ten amino acid long peptides and three peptides with L at position six and Y at position nine were identified ($Ro60_{323\text{-}332}$HVLIALETYR, $Ro60_{528\text{-}537}$ HPAVALREYR, and $Ro60_{270\text{-}279}$VEAEKLLKYL). The composition of each peptide with anchor residues at positions six and nine would ensure optimal binding to the MHC and presentation to the TCR.

2.3. Animal studies

NODShiLt/J mice were purchased from Jackson Laboratory (Bar Harbor, ME). Mice were allowed to acclimate to the facility for at least five days before handling. All animal experiments in these described studies were approved by the Institutional Animal Care and Use Committee at the University of Florida. All animals were maintained on a 12-h light-dark schedule and provided food and water ad libitum. Three cohorts of 6-week-old mice were injected with TATD ($n = 8$), 8-Aza (n = 8) (Combi Blocks, CA, USA), or PBS ($n = 6$) as controls. These drugs were injected at 20mgs/kg every day five days/week for 23 weeks in total. Saliva was collected first after nine weeks, 14 weeks, 16 weeks, 19 weeks, and 22 weeks of drug/vehicle injection. Tears were collected at three weeks and 19 weeks after the drug being injected. The treatment of the mice with TATD and 8-Aza was repeated twice with a similar number of animals to ensure the consistency of the results. Mice were anesthetized with isoflurane and euthanized by cervical dislocation, and their organs and tissues were freshly harvested for analysis.

2.4. Assessment of diabetes

Glucose was measured weekly with the AlphaTRAK 2 blood glucose monitoring system, and mice were considered diabetic after two consecutive blood glucose values of 250 mg/dl. Blood glucose levels were analyzed twice a week.

2.5. Measurement of saliva flow rate

To measure stimulated flow rates of saliva, individual mice were weighed and given an intraperitoneal (ip) injection of 100 μl of a mixture containing isoproterenol (0.2 mg/1 ml of PBS) and pilocarpine (0.05 mg/1 ml of PBS). Saliva was collected for 10 min from the oral cavity of individual mice using a micropipette starting 1 min after injection of isoproterenol and pilocarpine. The volume of each saliva sample was measured.

2.6. Measurement of tear flow

To measure stimulated tear flow, individual mice were weighed and given an intraperitoneal (ip) injection of pilocarpine (0.05 mg/1 ml of PBS). A phenol red thread is inserted next to the conjunctiva of the mouse after 1 min of the pilocarpine being injected, which indicates a colour change based on the quantity of tears produced. The length of the thread stained was recorded in millimeters (mm).

2.7. Response to Ro peptides by IL-2 secretion

Spleen cells were extracted from NOD mice and cultured in RPMI complete media with 100 μg/ml of the three peptides, namely mRo60$_{323\text{-}332}$HVLIALETYR, mRo60$_{528\text{-}537}$ HPAVALREYR, and mRo60$_{270\text{-}279}$VEAEKLLKYL or 100 μg/ml positive control B9:23 and 100 μg/ml negative control CLIP peptide at 37 °C for 24 h. All peptides were purchased and produced by GeneScript. The cultures were performed with Ro60 peptides with and without 100 mM TATD and 100 mM 8-Aza. 100 μl of cell supernatant was used to run an ELISA. ELISA Max standard set mouse IL-2 (BioLegend, #431001) was used to measure IL-2, and the assay was performed per the manufacturer's instructions.

2.8. ELISA for detecting the antibodies against Ro52, Ro60, and La

Recombinant mouse antibodies Ro52/SS-A (#12700), Ro60/SS-A (#15500), and La/SS-B (#12800, Diarect, Freiburg, Germany) were used to coat individual wells of a 96-well plate at a concentration of 0.6 μg/mL in carbonate buffer pH 9.6 overnight at 4 °C. The plate was washed with phosphate-buffered saline pH 7.4 with 0.05% Tween 20 (PBST), and then blocked-in phosphate-buffered saline pH 7.4 (PBS) with 5% bovine serum albumin overnight at 4 °C. 200 μL of a 1:20 dilution of sera was added into each well in triplicate. Sera from mice of both cohorts were incubated at room temperature for 2 h. The plate was then washed with PBST and treated with a 1:10,000 dilution of anti-mouse IgG (#SC-2005, Santa Cruz Biotech, Santa Cruz, California) conjugated to horseradish peroxidase (HRP) in PBS and incubated for 2 h at room temperature. After washing the plate with PBST, the wells were treated with 100uL of TMB substrate solution (#00–4201-56, eBioscience, San Diego, California) for 30 min with shaking and then with 3 N HCl to stop. The plate was read at an absorbance of 450 nm using Tecan Infinite M200 Pro spectrophotometric plate reader. The data was recorded as relative absorbance.

2.9. Histological examination of the salivary and lacrimal glands

Salivary and lacrimal glands of NOD ShiLt/J were fixed in 10% phosphate-buffered formalin for 48 h. Fixed tissues were embedded in paraffin and sectioned at a thickness of 5 μm. The prepared tissue sections were stained with hematoxylin and eosin (H&E) dye (Histology Tech Services, Gainesville, FL). Stained sections were observed at 10× magnification using Nikon Eclipse Ti-E inverted microscope, and representative images were recorded at 20×. To detect and determine leukocytic infiltrations in salivary glands, a single histological section per gland per mouse was examined by a blinded examiner. Lymphocytic infiltrations were defined as aggregates of >50 leukocytes in the entire gland.

2.10. Immunofluorescent staining for $CD3^+$T cells and $B220^+$B cells

Paraffin-embedded tissues of the salivary glands were sectioned and mounted onto microscope slides. According to the manufacturer's instructions, slides were deparaffinized and dehydrated by pressure-cooking in Trilogy (Cell Marque, Rocklin, CA). Following three 5-min washes with phosphate-buffered saline with Tween-20 (PBS-T) at 25 °C, the sections were incubated for 1 h with a blocking solution containing donkey serum diluted 1:50 in PBS-T. Each section was incubated with purified rat anti-mouse CD45R (Clone 30-F11, BD Pharmingen, San Jose, CA, USA) diluted 1:25 and goat polyclonal IgG anti-mouse CD3ε (Clone M-20, Santa Cruz Biotechnology, Santa Cruz, CA, USA) diluted 1:50 in antibody diluent (Dako, Carpinteria, CA, USA) for 1 h at 25 °C. The slides were washed three times with PBS-T, followed by a one-hour incubation with Alexa Fluor (AF) 488 donkey anti-goat IgG (H + L) diluted 1:100, and AF 594 donkey anti-rat IgG (H + L) (Life Technologies, Grand Island, NY, USA) diluted 1:25 at 25 °C. The slides were washed thoroughly with PBS-T, treated with Vectashield DAPI (4,6-diamidino-2-phenylindole)-mounting medium (Vector Laboratories, Burlingame, CA, USA), and overlaid with glass coverslips. Stained sections were visualized at 100× magnification on Nikon Ti-E fluorescent microscope. Infiltrate size and composition were calculated using Nikon NIS-Elements software at 20×

magnification, wherein infiltration areas were determined using the region of interest (ROI) established around the infiltrates.

2.11. Detection of anti-nuclear antibodies (ANA) in the sera

Anti-nuclear antibodies were detected in the sera of mice by using the HEp-2 ANA kit (Inova Diagnostics, Inc., San Diego, CA, USA). All procedures were performed according to the manufacturer's instructions. Mouse sera were diluted at 1:80 and incubated on HEp-2-fixed substrate slides for 1 h at room temperature in a humidified chamber. After three 5-min washes with PBS, the substrate slides were treated with a 1:100 dilution of AF 488 goat anti-mouse IgG (H + L) (Life Technologies) for 45 min at room temperature. After three washes, slides were treated with Vectashield DAPI-mounting medium (Vector Laboratories) and overlaid with glass coverslips. Fluorescence was detected by fluorescence microscopy at 20× magnification using a Nikon microscope, and all images were obtained with exposure of 200 milliseconds.

2.12. Flow cytometry

Salivary glands were digested in a digest buffer (1 mg/ml DNase (Sigma-Aldrich, St. Louis, MO, USA) and 1 mg/ml Collagenase Type 4 (Worthington, Lakewood, NJ, USA) in RPMI (Lonza, Allendale, NJ, USA) complete media containing 10% FBS, 2 mM L-glutamine, 0.05 mM β-mercaptoethanol) and placed in a MACS C tube (Miltenyi Biotec, San Diego, CA, USA) for desiccation on GentleMACS V1.02 for a pulse of 38 s, twice. After a 10-min incubation at 37 °C, the digest buffer was removed, placed into 4 °C RPMI complete media, and replaced with another digest buffer to repeat the process twice more. Single-cell suspensions were centrifuged (2500 rpm, 10 min, 4 °C) and resuspended in PBS for filtration through a 70-μm sterile cell strainer (Fisher, Pittsburgh, PA, USA). After a wash with PBS, cells were resuspended in PBS for lymphocyte isolation with Lympholyte-M cell separation media (Cedar Lane, Bulington, Ontario, Canada) per the manufacturer's instructions. Single-cell suspensions were stained for surface markers using the following stains: PE for CD3 (BD Bioscience catalog #553064), PerCP-Cy5.5 for CD4 (Biolegend catalog #116011), FITC for CD8 (BD Bioscience catalog # 553031), APC for IFN-Gamma (BD Bioscience catalog #552772), BV421 for IL-17(Biolegend catalog #505810), PE Cy7 for B220 (Biolegend catalog #506926), AmCyan as a live dead marker (ThermoFisher catalog #2031176). Lymphocytes were initially gated on forward and side scatter properties, followed by live cells markers. The cell populations were assessed for surface expression of $CD3^+$, $CD4^+$, $CD8^+$ and $B220^+$ cells. The samples were analyzed using BD Fortessa Flow Cytometer (BD Biosciences, San Jose, CA, USA), and analysis was performed using FlowJo VX software (FlowJo, Ashland, OR, USA).

2.13. Analysis of mouse serum cytokine levels

The serum cytokine levels were determined using the 8-plex-mouse cytokine group I Bioplex kit (BioRad, Hercules, CA) per the manufacturer's instruction. In brief, sera samples were diluted 1:4 in the provided assay buffer. A 96-well assay plate was prewet with 100 μl of assay buffer. Pre-mixed beads were added to each well in a 50 μl volume and then washed, using a magnet for bead retention, before adding 50 μl of the diluted sample, standard, or blank. The assay plate was incubated for 30 min by shaking at

room temperature in the dark. The plate was then washed before the addition of the detection antibody. Following the detection antibody, the plate was washed by adding 50 μl of Streptavidin-PE per well. The samples were incubated for 10 min by shaking. The plate was washed for the final time, and 125 μl of assay buffer was added. The results were acquired using BioRad Magpix. The data were analyzed using the Bio-Plex Manager software (BioRad, Hercules, CA).

2.14. Statistical analysis

All presented data are the mean ± standard error of the mean (SEM). Statistical significance was tested using GraphPad Prism 9 (Prism, Irvine, CA). Two-Way ANOVA with Fishers uncorrected LSD test was used. Unpaired students *t*-test and Mann-Whitney one-tailed *t*-tests were used to compare tear flow, ELISA for antibodies against Ro52, Ro60, and La, and cell counts as observed in flow cytometry. All results are discerned to the 95% confidence interval response.

3. Results

3.1. Determining the Ro60 antigenic epitopes to I—A^{g7} and the binding capacity of TATD and 8-Aza

NOD mice develop Type 1 Diabetes (T1D) and SjS independently [33]. The development of T1D in NOD mice is associated with the main MHC class II I—A^{g7} [34]. Moreover, the insulin B9:23 is the primary antigenic epitope presented by I—A^{g7} to initiate the onset of diabetes [21,35]. In SjS, several autoantigens have been implicated, for example, Ro60, Ro52, La, α-fodrin, and muscarinic acetylcholine 3 receptor (M3R) [36]. However, it has not been well defined if these antigens have the propensity to bind to the I—A^{g7} and elicit a T cell response. Furthermore, it remains unexplored whether previously characterized small molecules can interfere with the antigen-presenting process, affecting the T cell response. To examine these critical issues, we first used MHC binding prediction to map the antigenic epitopes of Ro60 with I—A^{g7}. Based on a previous study, which defined a sequence motif for the nine amino acid core of peptides that bind I-A^{g7}; with an anchor residue at position 6 (leucine preferred) and at position 9 (tyrosine preferred) [35]. We identified three ten amino acid long peptides of the Ro60 autoantigen with leucine and tyrosine at positions 6 and 9, respectively (HVLIALETYR, HPAVALREYR, and VEAEKLLKYL). Structural models of candidate autoantigen peptides show accommodation of leucine in the P6 pocket and tyrosine in the P9 pocket of I—A^{g7} (HVLIALETYR shown in Fig. 1A). Comparable structural binding was found with HPAVALREYR and VEAEKLLKYL peptides (data not shown).

Secondly, we sought to determine whether two previously characterized B9:23/I-A^{g7} blocking small molecules, TATD and 8-Aza, could interfere with Ro60/I-A^{g7} interaction. As presented in Fig. 1B, superposition with candidate autoantigen peptides (e.g., HVLIALETYR, Fig. 1A) showed that TATD and 8-Aza occupied sites involved in inter-molecular contact between the peptide and I—A^{g7}. Occupancy of a structural pocket in I—A^{g7} with TATD was predicted to sterically hinder glutamic acid (E) at position seven of Ro60 peptide ($Ro60_{323\text{-}332}$HVLIALETYR). We hypothesize that the I—A^{g7} binding

autoantigen peptides such as $Ro60_{323\text{-}332}$HVLIALETYR may inhibit binding the antigen-binding cleft with small molecules (Fig. 1C). TATD binding in the cleft would cause a steric clash with HVLIALETYR, as indicated in Fig. 1D.

Lastly, to further support the structural modeling results, we sought to determine whether the Ro60 peptides can stimulate NOD T cell response and examine the effect of TATD and 8-Aza on these responses. As presented in Fig. 1E, similar to the diabetic B9:23 epitope, $Ro60_{323\text{-}332}$HVLIALETYR, $Ro60_{528\text{-}537}$ HPAVALREYR elicited a robust T cell response, and the response was significantly diminished with TATD and 8-Aza. $Ro60_{270\text{-}279}$VEAEKLLKYL showed a lesser response; however, both small molecules were still able to reduce the proliferation of T cells, as a result decreasing the amount of IL-2. In summary, the data showed that structural modeling could identify antigenic epitopes of Ro60 binding to I—A^{g7} and the inhibitory effect of TATD and 8-Aza.

3.2. TATD and 8-Aza improved salivary and lacrimal secretory function in the NOD mice

The NOD mice develop SjS-like autoimmune exocrinopathy in which salivary and lacrimal gland infiltration occurs at 12–16 weeks of age, followed by secretory dysfunction by 16 weeks of age. The NOD mice also exhibited several signature autoantibodies of SjS by 24 weeks of age. To determine whether blocking I—A^{g7} can prevent the autoimmune response, we treated 6-week-old female NOD mice with TATD or 8-Aza at 20mgs/kg for five days a week for 22 weeks. As shown in Fig. 2A, 8-Aza-treated mice showed statistically signficiant increase in saliva flow rates (SFR) at 14, 19, and 22 weeks, but not 16 weeks post treatment compared to the PBS-treated mice. TATD-treated mice showed an increased trend of SFR after 9 weeks post treatment in comparison to PBS-treated mice at the same time interval, but the trend was not statistically signficiant. In addition, we sought to determine the effect of TATD and 8-Aza in tear secretion over the same 22-week time span. As presented in Fig. 2B, the TATD treated group showed an increase in tear production compared to the PBS-treated group at the 20-week time point as per the drug dosing regimen (mice aged 25 weeks). The results indicate that TATD and 8-Aza prevented the secretory dysfunction in the salivary glands. TATD showed significant improvement in tear production post 20 weeks of treatment, whereas 8-Aza showed minimal effect on tear secretion compared to the PBS-treated mice.

3.3. TATD and 8-Aza reduced the levels of autoantibodies in the NOD mice

SjS pathogenesis is characterized by high levels of circulating serum autoantibodies [37,38]. We sought to investigate whether TATD and 8-Aza could limit the anti-nuclear antibodies (ANA) production. As presented in Fig. 3A, 62.5% of mice in both TATD-and 8-Aza-treated cohorts were ANA negative, and 37.5% were positive for ANA. In contrast, 33.33% of PBS-treated mice were ANA negative, and 66.67% were ANA positive. In addition, TATD and 8-Aza also significantly reduced anti-Ro52 levels and with minor effect on anti-Ro60 (Fig. 3B). Anti-SSB/La levels were not affected by either drug. The data indicate that TATD and 8-Aza were able to reduce the levels of autoantibodies, specifically anti-Ro52

3.4. TATD and 8-Aza reduced lymphocytic infiltration in the salivary and lacrimal glands

To determine whether TATD and 8-Aza impacted the severity of sialadenitis and the cellular composition of the infiltrates, we sought to examine histological sections of the salivary and lacrimal glands. As presented in Fig. 4A, TATD and 8-Aza reduced the focal scores in the salivary glands; however, it was not statistically significant. The impact of the two small molecules was more striking in the lacrimal glands, in which 8-Aza was able to significantly reduce the focal scores compared to the PBS-treated mice (Fig. 4B). To further quantify the total area of lymphocytic infiltrates, we stained the glands for B and T cells. As presented in Fig. 5, the drug-treated mice showed a reduced area of infiltrates in the salivary (Fig. 5A) and lacrimal glands (Fig. 5B) compared to the control PBS-treated mice where only the reduction in the salivary glands was statistically significant.

Since only the salivary glands showed significant differences based on the inflammatory infiltrates, we further examined the various subsets of T cells in the salivary glands. As presented in Fig. 6A, TATD- and 8-Aza-treated mice showed a significant reduction in the $CD4^+$ T cells compared to PBS-treated mice. The Th1 and Th17 cell populations in the salivary glands were significantly reduced with both TATD and 8-Aza (Fig. 6B and C). In addition, TATD and 8-Aza reduced the frequency of $CD8^+$ T cells (Fig. 6D). Lastly, as presented in Fig. 6E, both drugs also significantly lowered B cells in the glands. Overall, TATD and 8-Aza reduced the severity of the sialadenitis by limiting the influx of B and T cells in the glands.

3.5. TATD and 8-Aza reduced key inflammatory cytokines

As demonstrated, we observed a general reduction of B cells and T cells with Th1 and Th17 subsets when mice were treated with TATD or 8-Aza. Next, we sought to determine if the diminishing numbers of inflammatory cell populations could also impact the cytokine levels. As shown in Fig. 7, TATD significantly reduced IL-2, IL-17, and IFN-γ levels. 8-Aza showed a decrease in IL-2, IL-5, and IL-17 levels. IL-4, IL-6, IL-12, and IL-13 levels were minimally affected by both small molecules. These results provide strong evidence to suggest that TATD and 8-Aza could negatively regulate or inhibit T cell response.

4. Discussion

SjS is characterized by the progression of inflammation in salivary and lacrimal glands characterized by an autoimmune attack, resulting in reduced secretion of tears and saliva [39]. It is challenging to develop an effective therapeutic for SjS since the symptoms are heterogeneous and mostly overlapping with other autoimmune diseases [8,40]. Hence, no specific therapeutic intervention available for SjS exists [40,41]. Most treatments are generic biologic immune suppressants and do not consider the genetic associations of the disease. To address this therapeutic concept, this study sought to evaluate the effect of two repurposed, FDA-approved drugs identified by a rational structure-based approach to block I-A^{g7} of the NOD mice. Here, we demonstrated that TATD and 8-Aza alleviated the salivary and lacrimal gland secretory function, reduced circulating autoantibodies, lessened sialadenitis by decreasing the frequency and size of lymphocytic foci, limiting the influx of effector T and B cells in the glands, and reduced key pro-inflammatory cytokines.

The NOD mouse is a preclinical model that mimics the onset of SjS in human patients. In the NOD model for T1D, the GAD 65 peptide was used to model the insulin B:9–23 B chain by superimposing the antigen-binding clefts of DQ8 and I—Ag7 to determine sites of critical contact between peptide and MHC [21]. The atomic coordinates of B:9–23 peptide and I—A^{g7} showed that the orientation and conformation of insulin B:9–23 were complementary to the binding cleft of I—A^{g7} [22]. Furthermore, by the analysis of peptides that were eluted from cell lines expressing I—A^{g7}, it was found that most eluted peptides contained acidic amino acids at the carboxy end, which were responsible for them being able to be presented on the I—A^{g7} [42]. Replacing histidine and serine at residues 56 and 57 with proline and aspartic acid, respectively, in the I—Ag^{7} beta chain prevented diabetes and eliminated stimulation of autoreactive T cells in the NOD mice [43]. Ro60 is one of the major autoantigens in SjS, and anti-Ro60 autoantibodies were found in the NOD mice, indicating the activation of autoreactive T and B cells by antigen-presenting cells expressing I—Ag^{7}. Based on the peptide composition that structurally fits best in the I—A^{g7} antigen-binding cleft, it was predicted that I—Ag^{7} should have the anchor residues of leucine at position six and tyrosine at position nine [35]. Scanning the entire Ro60 protein at ten amino acid segments, we identified three peptides ($Ro60_{323\text{-}332}$HVLIALETYR, $Ro60_{528–537}$ HPAVALREYR, and $Ro60_{270\text{-}279}$VEAEKLLKYL with leucine and tyrosine at positions 6 and 9 that would ensure optimal binding to the MHC and presentation to the TCR. The three unique ten amino acids long of Ro60 with nine amino acid core, specifically $Ro60_{323\text{-}332}$HVLIALETYR and $Ro60_{528–537}$ HPAVALREYR, elicited robust T cell response. Synthetic peptides with short amino acid length have been shown to bind to MHC class II molecules. However, natural ligands for MHC class II molecules are often longer, ranging from 13 to 17 amino acids [44–46]. The insulin B9:23 peptide is longer (15 amino acids) than the three Ro60 peptides and elicited a response that was higher than the three peptides. Therefore, it is possible that longer Ro60 peptides may generate stronger T cell responses. The effect of peptide length on MHC affinity remains to be determined; however, studies have demonstrated that the residues that flank the nine amino acid core can influence T cell response by increasing the binding affinity of peptides by non-specific interactions with MHC class II molecules [47–49]. Deshmukh et al. have shown that mouse Ro60 peptides from 281 to 300 and 311–330 showed high in-vitro T cell proliferative responses. These two peptides, including $Ro60_{519–538}$, elicited reactivity in SJL/J mice after immunization with recombinant mouse Ro60 with $mRo60_{311–330}$ being the most dominant peptide [50]. Moreover, immunization of the peptides produced peptide-specific antibodies that recognized the predominant T cell epitopes [50,51]. Our study identified three unique peptides that can potentially modulate the autoimmune response with high affinity to I—Ag^{7}.

The development of SjS is mediated by the complex interaction of many cell types at the predicted time intervals learned from the animal models [10]. Phase 1 (0–8 weeks) is characterized by acinar epithelial cell death and delayed gland morphogenesis. Phase 2 (8–16 weeks), where IFN stimulated genes to become activated, coincides with the migration of macrophages and dendritic cells (DCs), followed by $CD4^{+}$T and $B220^{+}$B lymphocytes emergence of autoantibodies. Finally, in Phase 3 (16 weeks onward), there is an overt clinical disease where a progressive measurable loss of exocrine gland function occurs.

Infiltrates primarily composed of $CD4^+$ T cells were discovered at 24 weeks of age [52]. Disrupting one or more steps of this disease cascade may alleviate SjS development. The activation of B and T cells is first involved in the autoantigen presentation by APC to activate T cells, followed by the clonal expansion of autoantibody-producing B cells. Based on this concept, targeting antigen presentation by blocking MHC molecules should stop the disease cascade, resulting in the mitigation of disease onset. As demonstrated in this study, blocking I—Ag^7 of the NOD mice using TATD and 8-Aza lowered Th1, Th17, $CD8^+$ T cells, and B cells in the glands. Both drugs reduced the levels of autoantibodies, sialadenitis and improved salivary and lacrimal secretory function.

Further, these drugs were able to decrease IL-5 and IL-17 in NOD mice. These findings are consistent with previous studies in which blocking I—Ag^7 prevented the T1D in NOD mice, and blocking DQ8 using Methyldopa reduced inflammatory T cell responses to insulin and T1D in patients [22]. A recent study by Li et al. showed that Cepharanthine, a compound that blocks HLA-DRβ1-Arg74, could prevent the presentation and T-cell responses to TSHR (thyroid-stimulating hormone receptor) in the experimental autoimmune Graves' disease model [23]. Another study has shown that copolymers blocking HLA-DR2 (DRB1*1501) prevented the progression of multiple sclerosis (MS) [53]. Therefore, targeting HLAs could be a viable approach to interfere with autoantigen recognition of autoreactive T cells. As demonstrated by our study, this method of interference could dampen the immune response and ameliorate the development of SjS.

There is currently no cure for SjS. 97% of patients report using eye drops, artificial tears, or non-prescription eye ointments for treatment [54]. Patients rely on anti-inflammatory agents such as disease-modifying anti-rheumatic drugs (DMARDs), Rituximab (anti-CD20), and corticosteroids [40,55,56]. Other drugs, including hydroxychloroquine (HCQ), methotrexate, and azathioprine, provided mixed results in clinical trials [57–59]. These therapies do not take into account the genetic component of the disease [60]. This study describes a novel approach to identifying small immunomodulatory molecules targeting HLA for SjS. The ability to identify HLA allele-specific drugs has broad applicability for treating autoimmune diseases and other HLA-associated diseases with applications in personalized medicine. Thus, this study emphasizes that rare autoimmune therapy can halt the autoimmune cascade rather than treating symptoms.

Acknowledgments

We thanked Dr. Aaron Michels for generously providing TATD for the study. CQN is supported financially in part by PHS grants AI130561, DE026450, and DE028544 from the National Institutes of Health.

References

[1]. Helmick CG, Felson DT, Lawrence RC, Gabriel S, Hirsch R, Kwoh CK, Estimates of the prevalence of arthritis and other rheumatic conditions in the United States. Part I, Arthritis Rheum. 58 (1) (2008) 15–25. [PubMed: 18163481]

[2]. Reksten TR, Jonsson MV, Sjögren's syndrome: an update on epidemiology and current insights on pathophysiology, Oral Maxillofac. Surg. Clin. North Am 26 (1) (2014) 1–12. [PubMed: 24287189]

[3]. Priori R, Minniti A, Derme M, Antonazzo B, Brancatisano F, Ghirini S, et al. , Quality of sexual life in women with primary Sjögren syndrome, J. Rheumatol 42 (8) (2015) 1427–1431. [PubMed: 26136488]

[4]. Pierce JL, Tanner K, Merrill RM, Miller KL, Kendall KA, Roy N, Swallowing disorders in Sjögren's syndrome: prevalence, risk factors, and effects on quality of life, Dysphagia 31 (1) (2016) 49–59. [PubMed: 26482060]

[5]. Akpek EK, Mathews P, Hahn S, Hessen M, Kim J, Grader-Beck T, et al. , Ocular and systemic morbidity in a longitudinal cohort of Sjögren's syndrome, Ophthalmology 122 (1) (2015) 56–61. [PubMed: 25178806]

[6]. Moerman RV, Bootsma H, Kroese FG, Vissink A, Sjogren's syndrome in older patients: aetiology, diagnosis and management, Drugs Aging 30 (3) (2013) 137–153. [PubMed: 23341116]

[7]. Ekstrom Smedby K, Vajdic CM, Falster M, Engels EA, Martinez-Maza O, Turner J, et al. , Autoimmune disorders and risk of non-hodgkin lymphoma subtypes: a pooled analysis within the InterLymph consortium, Blood 111 (8) (2008) 4029–4038. [PubMed: 18263783]

[8]. Fox RI, Sjogren's syndrome, Lancet 366 (9482) (2005) 321–331. [PubMed: 16039337]

[9]. Voigt A, Sukumaran S, Nguyen CQ, Beyond the glands: an in-depth perspective of neurological manifestations in Sjögren's syndrome, Rheumatology (Sunnyvale) 2014 (2014).

[10]. Witas R, Gupta S, Nguyen CQ, Contributions of major cell populations to Sjögren's syndrome, J. Clin. Med 9 (9) (2020).

[11]. Sakai A, Sugawara Y, Kuroishi T, Sasano T, Sugawara S, Identification of IL-18 and Th17 cells in salivary glands of patients with Sjogren's syndrome, and amplification of IL-17-mediated secretion of inflammatory cytokines from salivary gland cells by IL-18, J. Immunol 181 (4) (2008) 2898–2906. [PubMed: 18684981]

[12]. Voigt A, Esfandiary L, Nguyen CQ, Sexual dimorphism in an animal model of Sjögren's syndrome: a potential role for Th17 cells, Biol. Open 4 (11) (2015) 1410–1419. [PubMed: 26453623]

[13]. Katsifis GE, Rekka S, Moutsopoulos NM, Pillemer S, Wahl SM, Systemic and local interleukin-17 and linked cytokines associated with Sjögren's syndrome immunopathogenesis, Am. J. Pathol 175 (3) (2009) 1167–1177. [PubMed: 19700754]

[14]. Kyriakidis NC, Kapsogeorgou EK, Tzioufas AG, A comprehensive review of autoantibodies in primary Sjogren's syndrome: clinical phenotypes and regulatory mechanisms, J. Autoimmun 51 (2014) 67–74. [PubMed: 24333103]

[15]. Iizuka M, Tsuboi H, Matsuo N, Kondo Y, Asashima H, Matsui M, et al. , The crucial roles of IFN-γ in the development of M3 muscarinic acetylcholine receptor induced Sjögren's syndrome-like sialadenitis, Mod. Rheumatol 23 (3) (2013) 614–616. [PubMed: 23099472]

[16]. Voigt A, Bohn K, Sukumaran S, Stewart CM, Bhattacharya I, Nguyen CQ, Unique glandular ex-vivo Th1 and Th17 receptor motifs in Sjogren's syndrome patients using single-cell analysis, Clin. Immunol 192 (2018) 58–67. [PubMed: 29679709]

[17]. Nguyen CQ, Hu MH, Li Y, Stewart C, Peck AB, Salivary gland tissue expression of interleukin-23 and interleukin-17 in Sjögren's syndrome: findings in humans and mice, Arthritis Rheum. 58 (3) (2008) 734–743. [PubMed: 18311793]

[18]. Lin X, Rui K, Deng J, Tian J, Wang X, Wang S, et al. , Th17 cells play a critical role in the development of experimental Sjögren's syndrome, Ann. Rheum. Dis 74 (6) (2015) 1302. [PubMed: 24573745]

[19]. Wanchoo A, Voigt A, Sukumaran S, Stewart CM, Bhattacharya I, Nguyen CQ, Single-cell analysis reveals sexually dimorphic repertoires of interferon-γ and IL-17A producing T cells in salivary glands of Sjögren's syndrome mice, Sci. Rep 7 (1) (2017) 12512. [PubMed: 28970488]

[20]. Nguyen CQ, Yin H, Lee BH, Carcamo WC, Chiorini JA, Peck AB, Pathogenic effect of interleukin-17A in induction of Sjögren's syndrome-like disease using adenovirus-mediated gene transfer, Arthritis Res. Ther 12 (6) (2010) R220. [PubMed: 21182786]

[21]. Michels AW, Ostrov DA, Zhang L, Nakayama M, Fuse M, McDaniel K, et al. , Structure-based selection of small molecules to alter allele-specific MHC class II antigen presentation, J. Immunol 187 (11) (2011) 5921–5930. [PubMed: 22043012]

[22]. Ostrov DA, Alkanani A, McDaniel KA, Case S, Baschal EE, Pyle L, et al. , Methyldopa blocks MHC class II binding to disease-specific antigens in autoimmune diabetes, J. Clin. Invest 128 (5) (2018) 1888–1902. [PubMed: 29438107]

[23]. Li CW, Osman R, Menconi F, Concepcion E, Tomer Y, Cepharanthine blocks TSH receptor peptide presentation by HLA-DR3: therapeutic implications to Graves' disease, J. Autoimmun 108 (2020), 102402. [PubMed: 31980336]

[24]. Li CW, Menconi F, Osman R, Mezei M, Jacobson EM, Concepcion E, et al. , Identifying a small molecule blocking antigen presentation in autoimmune thyroiditis, J. Biol. Chem 291 (8) (2016) 4079–4090. [PubMed: 26703475]

[25]. Cruz-Tapias P, Rojas-Villarraga A, Maier-Moore S, Anaya JM, HLA and Sjogren's syndrome susceptibility. A meta-analysis of worldwide studies, Autoimmun. Rev 11 (4) (2012) 281–287. [PubMed: 22001416]

[26]. Lessard CJ, Li H, Adrianto I, Ice JA, Rasmussen A, Grundahl KM, et al. , Variants at multiple loci implicated in both innate and adaptive immune responses are associated with Sjogren's syndrome, Nat. Genet 45 (11) (2013) 1284–1292. [PubMed: 24097067]

[27]. Harley JB, Reichlin M, Arnett FC, Alexander EL, Bias WB, Provost TT, Gene interaction at HLA-DQ enhances autoantibody production in primary Sjogren's syndrome, Science 232 (4754) (1986) 1145–1147. [PubMed: 3458307]

[28]. Gottenberg JE, Busson M, Loiseau P, Cohen-Solal J, Lepage V, Charron D, et al. , In primary Sjogren's syndrome, HLA class II is associated exclusively with autoantibody production and spreading of the autoimmune response, Arthritis Rheum. 48 (8) (2003) 2240–2245. [PubMed: 12905478]

[29]. Mohammed K, Pope J, Le Riche N, Brintnell W, Cairns E, Coles R, et al. , Association of severe inflammatory polyarthritis in primary Sjogren's syndrome: clinical, serologic, and HLA analysis, J. Rheumatol 36 (9) (2009) 1937–1942. [PubMed: 19487261]

[30]. Emsley P, Lohkamp B, Scott WG, Cowtan K, Features and development of coot, Acta Crystallogr. D Biol. Crystallogr 66 (Pt 4) (2010) 486–501. [PubMed: 20383002]

[31]. Liebschner D, Afonine PV, Baker ML, Bunkóczi G, Chen VB, Croll TI, et al. , Macromolecular structure determination using X-rays, neutrons and electrons: recent developments in phenix, Acta Crystallogr. D Struct. Biol 75 (Pt 10) (2019) 861–877. [PubMed: 31588918]

[32]. Morris GM, Huey R, Lindstrom W, Sanner MF, Belew RK, Goodsell DS, et al. , AutoDock4 and AutoDockTools4: automated docking with selective receptor flexibility, J. Comput. Chem 30 (16) (2009) 2785–2791. [PubMed: 19399780]

[33]. Nguyen CQ, Sharma A, Lee BH, She JX, McIndoe RA, Peck AB, Differential gene expression in the salivary gland during development and onset of xerostomia in Sjogren's syndrome-like disease of the C57BL/6.NOD-Aec1Aec2 mouse, Arthritis Res. Ther 11 (2) (2009), R56. [PubMed: 19379516]

[34]. Wen L, Wong FS, Sherwin R, Mora C, Human DQ8 can substitute for murine I-Ag7 in the selection of diabetogenic T cells restricted to I-Ag7, J. Immunol 168 (7) (2002) 3635–3640. [PubMed: 11907129]

[35]. Harrison LC, Honeyman MC, Trembleau S, Gregori S, Gallazzi F, Augstein P, et al. , A peptide-binding motif for I-A(g7), the class II major histocompatibility complex (MHC) molecule of NOD and Biozzi AB/H mice, J. Exp. Med 185 (6) (1997)1013–1021. [PubMed: 9091575]

[36]. Fye KH, Terasaki PI, Moutsopoulos H, Daniels TE, Michalski JP, Talal N, Association of Sjögren's syndrome with HLA-B8, Arthritis Rheum. 19 (5) (1976) 883–886. [PubMed: 962969]

[37]. Lavoie TN, Lee BH, Nguyen CQ, Current concepts: mouse models of Sjögren's syndrome, J. Biomed. Biotechnol 2011 (2011), 549107. [PubMed: 21253584]

[38]. Park YS, Gauna AE, Cha S, Mouse models of primary Sjogren's syndrome, Curr. Pharm. Des 21 (18) (2015) 2350–2364. [PubMed: 25777752]

[39]. Soliotis FC, Moutsopoulos HM, Sjogren's syndrome, Autoimmunity 37 (4) (2004) 305–307. [PubMed: 15518047]

[40]. Fox RI, Fox CM, Gottenberg JE, Dörner T, Treatment of Sjögren's syndrome: current therapy and future directions, Rheumatology (Oxford) 60 (5) (2021) 2066–2074, 10.1093/rheumatology/kez142. [PubMed: 31034046]

[41]. Nair JJ, Singh TP, Sjogren's syndrome: review of the aetiology, pathophysiology & potential therapeutic interventions, J Clin Exp Dent 9 (4) (2017) e584–e589. [PubMed: 28469828]

[42]. Suri A, Vidavsky I, van der Drift K, Kanagawa O, Gross ML, Unanue ER, In APCs, the autologous peptides selected by the diabetogenic I-Ag7 molecule are unique and determined by the amino acid changes in the P9 pocket, J. Immunol 168 (3) (2002) 1235–1243. [PubMed: 11801660]

[43]. Quartey-Papafio R, Lund T, Chandler P, Picard J, Ozegbe P, Day S, et al. , Aspartate at position 57 of nonobese diabetic I-Ag7 beta-chain diminishes the spontaneous incidence of insulin-dependent diabetes mellitus, J. Immunol 154 (10) (1995) 5567–5575. [PubMed: 7730655]

[44]. Rudensky Y, Preston-Hurlburt P, Hong SC, Barlow A, Janeway CA Jr., Sequence analysis of peptides bound to MHC class II molecules, Nature 353 (6345) (1991) 622–627. [PubMed: 1656276]

[45]. Andreatta M, Nielsen M, Characterizing the binding motifs of 11 common human HLA-DP and HLA-DQ molecules using NNAlign, Immunology 136 (3) (2012) 306–311. [PubMed: 22352343]

[46]. Chicz RM, Urban RG, Lane WS, Gorga JC, Stern LJ, Vignali DA, et al. , Predominant naturally processed peptides bound to HLA-DR1 are derived from MHC-related molecules and are heterogeneous in size, Nature 358 (6389) (1992) 764–768. [PubMed: 1380674]

[47]. O'Brien C, Flower DR, Feighery C, Peptide length significantly influences in vitro affinity for MHC class II molecules, Immunome Res. 4 (2008) 6. [PubMed: 19036163]

[48]. Cole DK, Gallagher K, Lemercier B, Holland CJ, Junaid S, Hindley JP, et al. , Modification of the carboxy-terminal flanking region of a universal influenza epitope alters CD4+ T-cell repertoire selection, Nat. Commun 3 (2012) 665. [PubMed: 22314361]

[49]. Sant'Angelo DB, Robinson E, Janeway CA Jr., Denzin LK, Recognition of core and flanking amino acids of MHC class II-bound peptides by the T cell receptor, Eur. J. Immunol 32 (9) (2002) 2510–2520. [PubMed: 12207335]

[50]. Deshmukh US, Lewis JE, Gaskin F, Kannapell CC, Waters ST, Lou YH, et al. , Immune responses to Ro60 and its peptides in mice. I. The nature of the immunogen and endogenous autoantigen determine the specificities of the induced autoantibodies, J. Exp. Med 189 (3) (1999) 531–540. [PubMed: 9927515]

[51]. Szymula A, Rosenthal J, Szczerba BM, Bagavant H, Fu SM, Deshmukh US, T cell epitope mimicry between Sjögren's syndrome Antigen A (SSA)/Ro60 and oral, gut, skin and vaginal bacteria, Clin. Immunol 152 (1–2) (2014) 1–9. [PubMed: 24576620]

[52]. Turpie B, Yoshimura T, Gulati A, Rios JD, Dartt DA, Masli S, Sjogren's syndrome-like ocular surface disease in thrombospondin-1 deficient mice, Am. J. Pathol 175 (3) (2009) 1136–1147. [PubMed: 19700744]

[53]. Fridkis-Hareli M, Design of peptide immunotherapies for MHC Class-II-associated autoimmune disorders, Clin. Dev. Immunol 2013 (2013), 826191. [PubMed: 24324511]

[54]. Stefanski AL, Tomiak C, Pleyer U, Dietrich T, Burmester GR, Dörner T, The diagnosis and treatment of Sjögren's Syndrome, Dtsch. Arztebl. Int 114 (20) (2017) 354–361. [PubMed: 28610655]

[55]. Vivino FB, Carsons SE, Foulks G, Daniels TE, Parke A, Brennan MT, et al. , New treatment guidelines for Sjögren's disease, Rheum. Dis. Clin. N. Am 42 (3) (2016) 531–551.

[56]. Ciccia F, Guggino G, Rizzo A, Alessandro R, Carubbi F, Giardina A, et al. , Rituximab modulates IL-17 expression in the salivary glands of patients with primary Sjögren's syndrome, Rheumatology (Oxford) 53 (7) (2014) 1313–1320. [PubMed: 24602921]

[57]. Skopouli FN, Jagiello P, Tsifetaki N, Moutsopoulos HM, Methotrexate in primary Sjögren's syndrome, Clin. Exp. Rheumatol 14 (5) (1996) 555–558. [PubMed: 8913659]

[58]. Gottenberg JE, Ravaud P, Puéchal X, Le Guern V, Sibilia J, Goeb V, et al. , Effects of hydroxychloroquine on symptomatic improvement in primary Sjögren syndrome: the JOQUER randomized clinical trial, JAMA 312 (3) (2014) 249–258. [PubMed: 25027140]

[59]. Price EJ, Rigby SP, Clancy U, Venables PJ, A double blind placebo controlled trial of azathioprine in the treatment of primary Sjögren's syndrome, J. Rheumatol 25 (5) (1998) 896–899. [PubMed: 9598887]

[60]. Verstappen GM, Kroese FGM, Bootsma H, T cells in primary Sjögren's syndrome: targets for early intervention, Rheumatology (Oxford) 60 (7) (2019) 3088–3098.

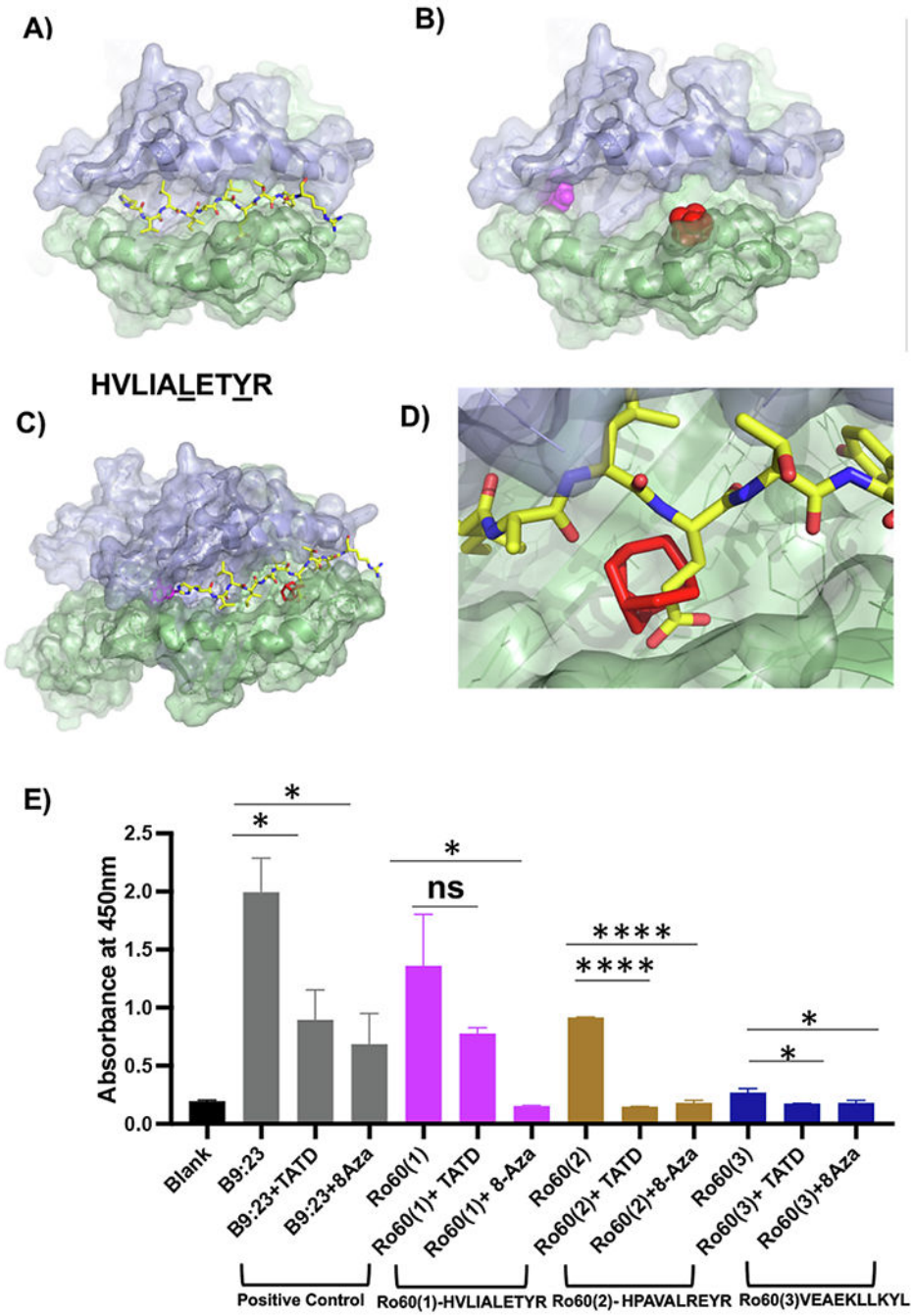

Fig. 1.

Structural modeling of a candidate autoantigen peptide and drug-like small molecules with I—A^{g7} A) $Ro60_{323\text{-}332}$HVLIALETYR, a peptide corresponding to murine Ro60, is shown as sticks modeled with I—A^{g7} (PDB code 6BLX); yellow for carbon, blue for nitrogen, red for oxygen. The α-chain of I—A^{g7} is shown in violet, β-chain in green. B) 8-Aza (magenta) and TATD (red) are shown as spheres in the top-scoring orientation posed by AutoDock Vina to the I—A^{g7} antigen-binding cleft. C) Superposition of $Ro60_{323\text{-}332}$HVLIALETYR on the I—A^{g7} antigen-binding cleft in the presence of 8-azaguanine (magenta sticks) and TATD

(red sticks). D) Steric clash between TATD and $Ro60_{323\text{-}332}$HVLIALETYR provides a strategy to inhibit autoantigen peptide presentation. E) Measurement of IL-2 by absorbance. For consistency, the experiment was performed in triplicate and repeated twice. Splenocytes were stimulated with HVLIALETYR, HPAVALREYR, and VEAEKLLKYL for 24 h with and without TATD and 8-Aza. Cultured supernatants were collected to assay for IL-2 levels. The statistical differences between control and drug-injected mice were determined using a one-way ANOVA with an uncorrected Fisher's LSD test at all threshold events. Error bars indicate with 95% class interval confidence, *: $p < 0.0332$, **: $p < 0.0021$, ***$p < 0.0002$, ****$p < 0.0001$, NS, not significant. (For interpretation of the references to colour in this figure legend, the reader is referred to the web version of this article.)

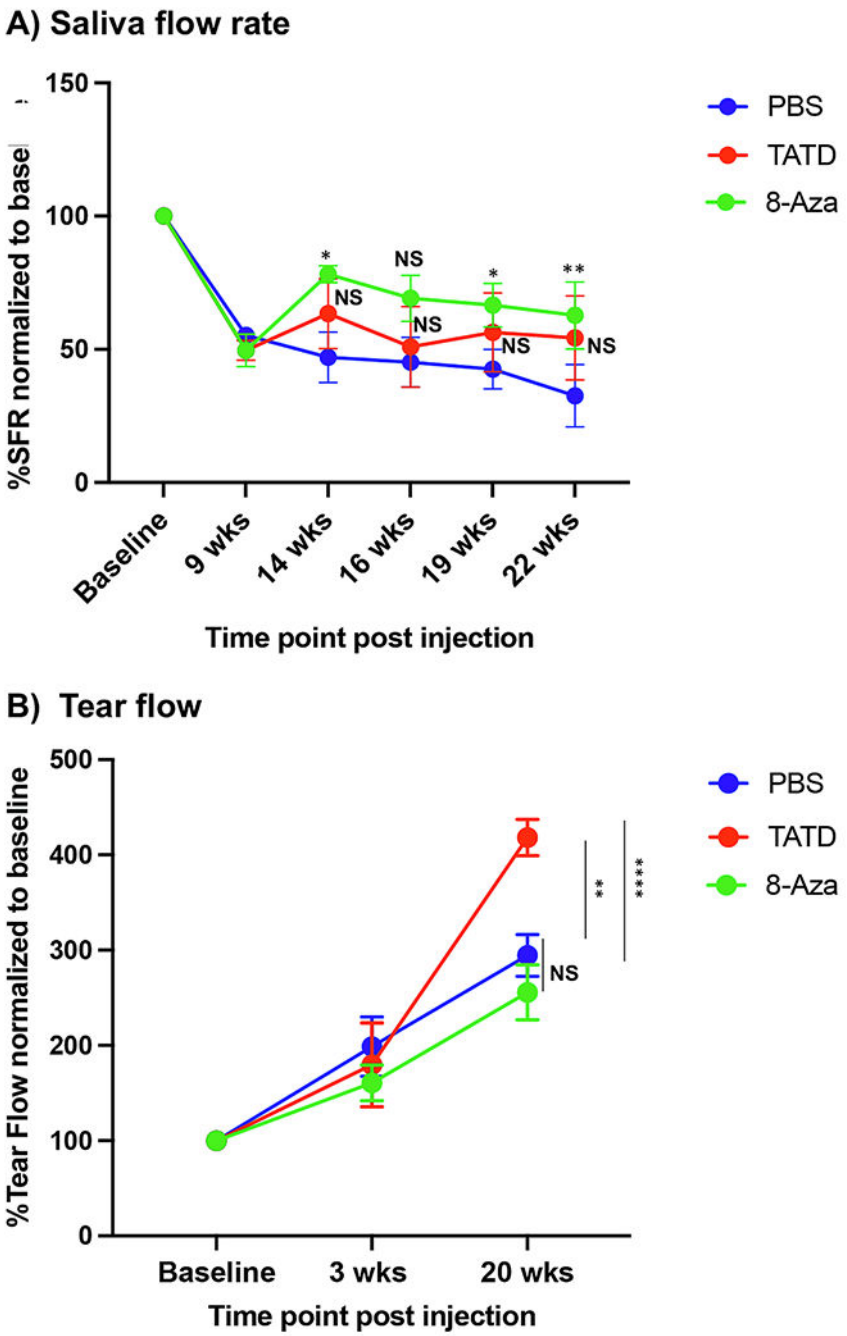

Fig. 2.

TATD and 8-Azaguanine improved saliva and tear production. A) Saliva flows were collected as described in the materials and methods section. The data shown represent the percentage of the SFR of TATD- (n = 8), 8-Aza-treated (n = 8), and PBS-treated (n = 6) normalized to the baseline (before drug treatment). B) Tear collection was performed as described in the materials and methods section. The data shown represents the tear collection on a phenol red thread for TATD (n = 8), 8-Aza-treated (n = 8) mice, and PBS-treated mice (n = 6). The statistical differences between PBS-treated versus TATD-treated or PBS-treated

versus 8-Aza-treated mice at specific age group were determined using unpaired *t*-test with 95% CI. *$p \leq 0.05$, **$p \leq 0.01$, ****$p \leq 0.0001$, NS, not significant. (For interpretation of the references to colour in this figure legend, the reader is referred to the web version of this article.)

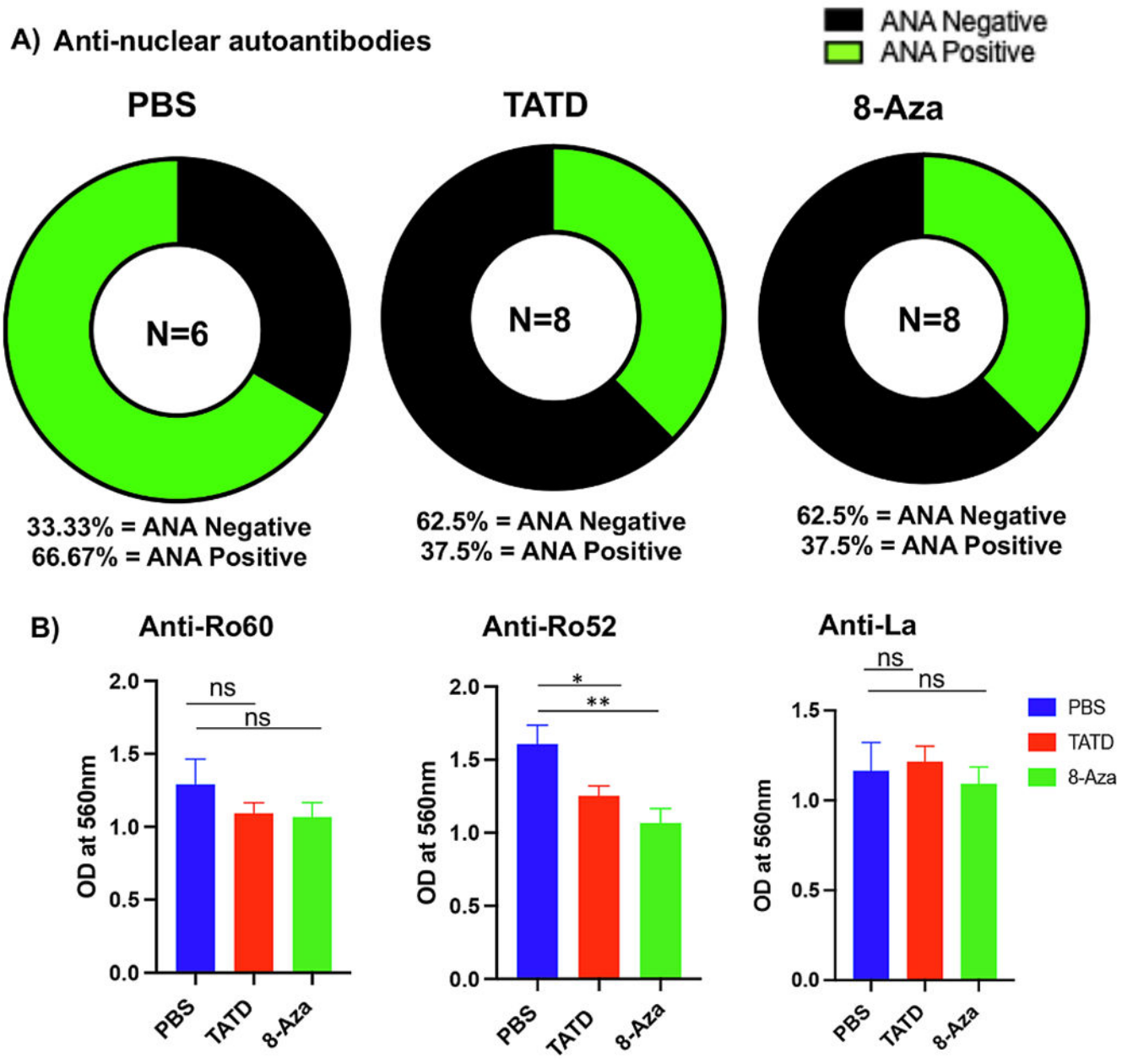

Fig. 3.

TATD and 8-Aza reduced autoantibodies in the NOD mice. A) ANA staining using HEp2 cells with TATD- (n = 8), 8-Aza- (n = 8), and PBS-treated (n = 6). The circular graphs displayed the frequency of animals with ANA negative or positive. B) Autoantibodies against Ro60, Ro52, and La were determined using ELISA. The statistical differences between control and drug-injected mice were determined using a one-way ANOVA with an uncorrected Fisher's LSD test at all threshold events. Error bars indicate with 95% class interval confidence, *: $p < 0.0332$, **: $p < 0.0021$, NS, not significant.

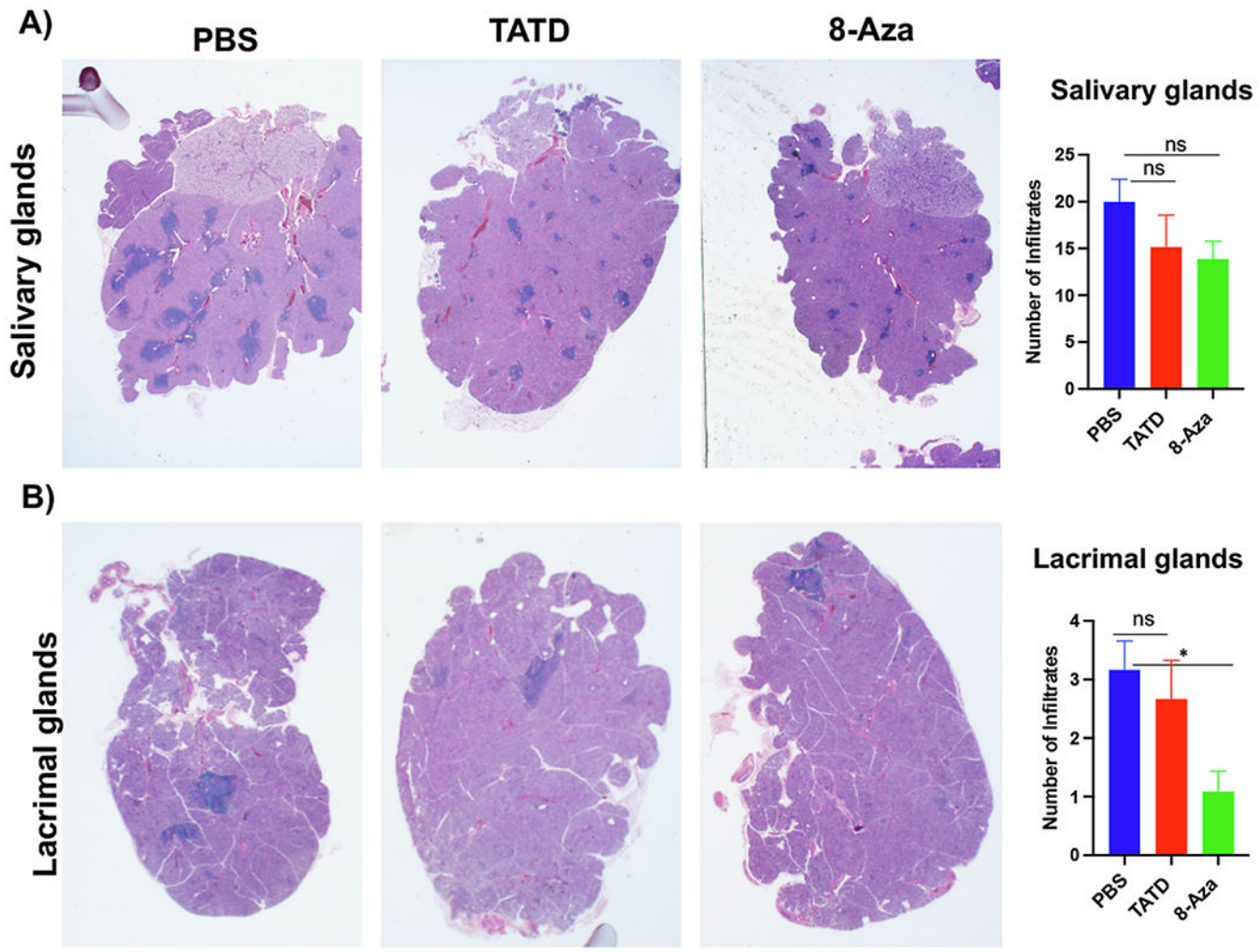

Fig. 4.

TATD and 8-Aza reduced lymphocytic infiltrations in the salivary and lacrimal glands. Salivary and lacrimal glands of female mice (TATD- (n = 8), 8-Aza-treated (n = 8) mice, and PBS-treated mice (n = 6)) were excised at the endpoint (27 weeks of age). Glands were stained with H&E. Representative images were presented at 20× magnification. To detect and determine leukocytic infiltrations, a single histological section per gland per mouse was examined by three blinded examiners. Lymphocytic infiltrations were defined as aggregates of >50 leukocytes. A) Salivary glands. B) Lacrimal glands. The statistical differences between control and drug-injected mice were determined using a one-way ANOVA with an uncorrected Fisher's LSD test at all threshold events. Error bars indicate with 95% class interval confidence, *: $p < 0.0332$, NS, not significant.

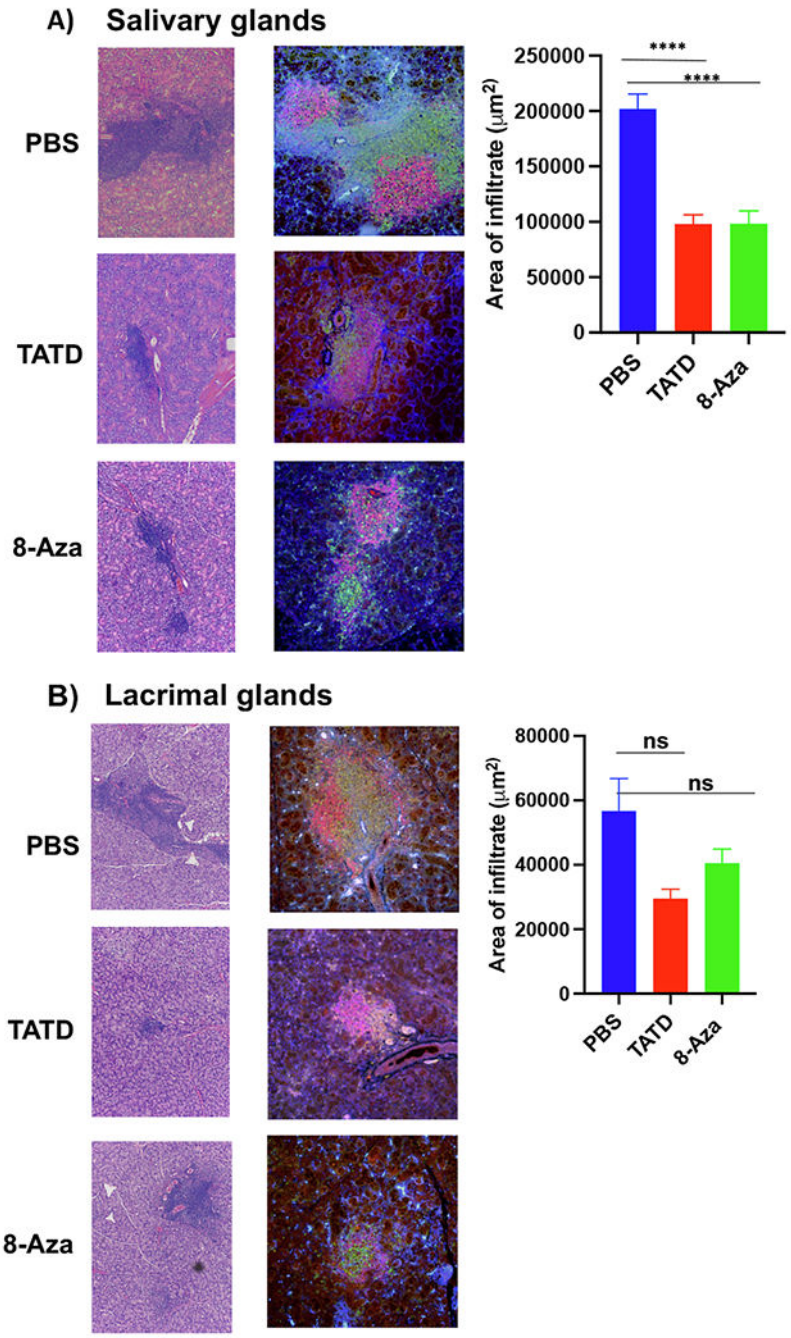

Fig. 5.

TATD and 8-Aza reduced the severity of lymphocytic infiltrations in the salivary and lacrimal glands. Based on immunofluorescent staining for CD3/B220 in TATD- (n = 8), 8-Aza- (n = 6) mice and PBS-treated mice (n = 6) mice, measurement of areas using densitometrical analysis was calculated using Nikon Elements software with the percentage of threshold events in ROI function. The mean ± standard of errors (SEM) was calculated for both the B and T cells. A) Salivary glands. B) Lacrimal glands. Representative images are shown at 20× magnification. The statistical differences between control and drug-injected

mice were determined using a one-way ANOVA with an uncorrected Fisher's LSD test at all threshold events. Error bars indicate with 95% class interval confidence, ****$p < 0.0001$, NS, not significant.

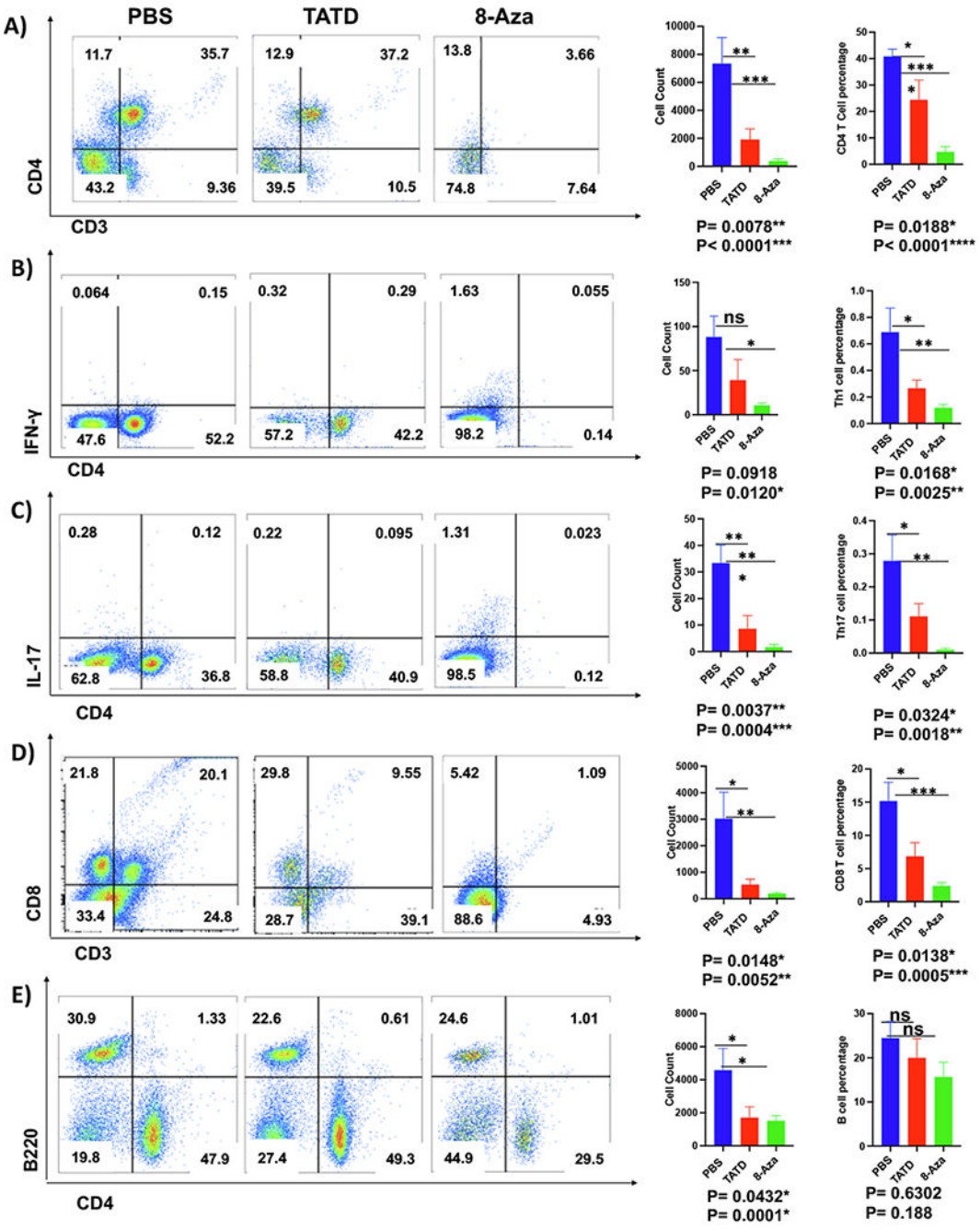

Fig. 6.

Reduction of the inflammatory cells in the salivary glands affected by TATD and 8-Aza. Glands were excised, and single-cell suspensions were isolated from TATD- (n = 8), 8-Aza- (n = 6) mice, and PBS-treated mice (n = 6) mice at 27 weeks of age. Flow cytometric acquisition was performed, and data analysis was performed using FlowJo software. Representative flow images, average cell count, and percentage with each group's standard of error bars were presented. A) $CD4^+$T cells. B) Th1 cells. C) Th17 cells. D) $CD8^+$ T cells. E) $B220^+$ B cells. The statistical differences between control and drug-injected mice were

determined using a one-way ANOVA with an uncorrected Fisher's LSD test at all threshold events. Error bars indicate with 95% class interval confidence, *: $p < 0.0332$, **: $p < 0.0021$, ***$p < 0.0002$, ****p < 0.0001, NS, not significant.

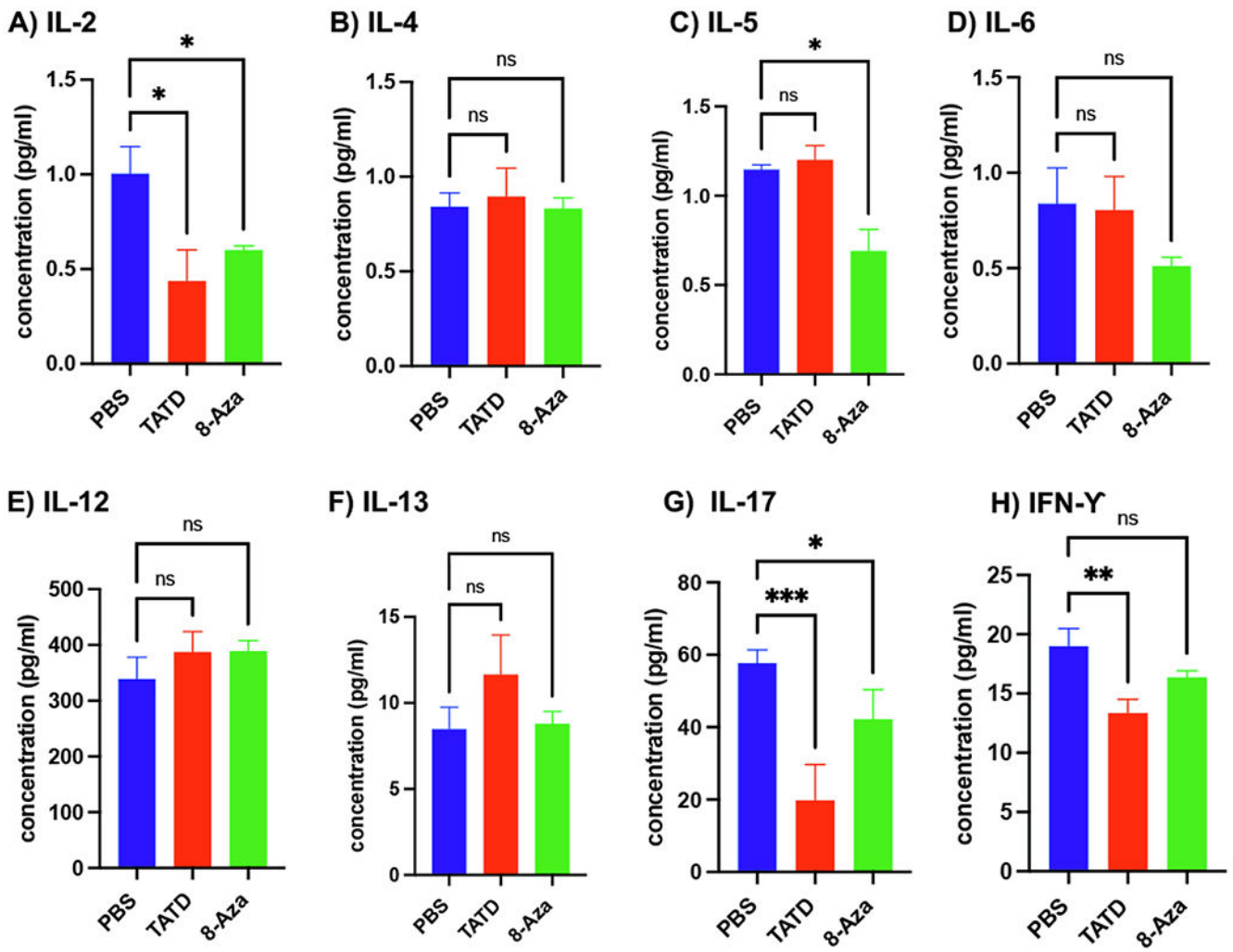

Fig. 7.

TATD and 8-Aza effects on systemic cytokine levels. A) IL-2, B) IL-4, C) IL-5, D) IL-6, E) IL-12, F) IL-13, G) IL-17, H) IFN-γ. Cytokine levels for TATD- (n = 8), 8-Aza-(n = 8), and PBS-treated mice (n = 6) were measured using the MagPix Assay. For consistency, the experiment was performed in triplicate and repeated twice. The statistical differences between control and drug-injected mice were determined using a one-way ANOVA with an uncorrected Fisher's LSD test at all threshold events. Error bars indicate with 95% class interval confidence, *: $p < 0.0332$, **: $p < 0.0021$, ***$p < 0.0002$, NS, not significant.